

MACHINE LEARNING-BASED MODEL ORDER REDUCTION FOR THE GUST LOAD  
ANALYSIS

**Sangmin Lee<sup>1</sup>, SiHun Lee<sup>2</sup>, Younggeun Park<sup>1</sup>, Seung-Hoon Kang<sup>1</sup>, Kijoo Jang<sup>2</sup>,  
Haeseong Cho<sup>3</sup>, SangJoon Shin<sup>1</sup>**

<sup>1</sup> Seoul National University  
Seoul, 08826, Republic of Korea  
sj7714@snu.ac.kr  
pyk31213@snu.ac.kr  
shkang94@snu.ac.kr  
ssjoon@snu.ac.kr

<sup>2</sup> Samsung Electronics Company  
Suwon-si, Gyeonggi-do, 16677, Republic of Korea  
s.hun.lee@samsung.com  
prastins@samsung.com

<sup>3</sup> Jeonbuk National University  
Jeonju-si, Jeollabuk-do, 54896, Republic of Korea  
hcho@jbnu.ac.kr

**Keywords:** Machine learning, nonlinear parametric model order reduction, gust load analysis

**Abstract:** This paper presents an efficient nonlinear non-intrusive model order reduction (MOR) framework for the gust load analysis. The proposed method is based on artificial neural network (ANN), specifically a least-square hierarchical variational autoencoder (LSH-VAE). This approach will enable construction of nonlinear reduced-order model and allow accurate interpolation with regard to the parameters. The proposed method will be validated by applying for a high-altitude long-endurance (HALE) unmanned aerial vehicle (UAV). The accuracy and computational efficiency of the method will be compared against those by a full order model (FOM). It is found that the proposed method will construct accurate interpolated field with regard to the relevant parameters.

## 1 INTRODUCTION

During the past few decades, research on unmanned fixed-wing aircraft capable of effectively performing various missions, such as surveillance and weather observation, has been pursued. Those UAV employ lightweight and flexible composite material-based high aspect-ratio wing, which offers improved aerodynamic efficiency and lift-to-drag ratio. However, those advantages are accompanied by reduction in structural integrity. In particular, when subjected to external forces such as gusts, the loads may vary instantaneously, resulting in severe structural deflection or vibration.

Within mission characteristics of UAV, high endurance performance will be a requirement. It is sufficiently likely that UAV will operate in environments with severe gust. Thus, it is of paramount

importance to involve pertinent analysis into the design process. Federal Aviation Regulations (FAR) [1] and European Aviation Safety Agency (EASA) [2] have established 1-cosine (one minus cosine) gust profile as a significant criterion for determining the gust load. The discrete gust profile comprises a number of the parameters, including gust strength and alleviation factor. To ensure aircraft safety during the design process, it will be necessary to consider possible values of those parameters in an iterative process.

The most preferred methodology for gust analysis comprises of the following two principal steps. The first step is to perform the aerodynamic analysis may be by the doublet lattice method (DLM). The second step is to conduct structural analysis by using the finite element method (FEM). Fluid-structure interaction analysis will require substantial computational time. Furthermore, in order to achieve an optimal design, it will be required to perform multi-query analysis across a range of the parameters. It will again lead to a significant amount of computational time and resource. As a substitute, MOR will be proposed to reduce the computational burden along with sufficient accuracy.

The non-intrusive MOR (NIMOR) involves the construction of a reduced model based on a set of input-output pair, allowing the aircraft properties to be included. Such approach will offer advantage of robustness and efficiency over an intrusive MOR. The robustness will be achieved by the separation of the stages into FOM scheme within the method and recovery of the reduced-basis solution [3]. NIMOR will become efficient because the reduced coefficients are obtained via evaluating the interpolation approach [4].

NIMOR is closely related to machine learning (ML), as it is dependent on the specific result. ML has been successfully applied for aerospace engineering field [5-7]. A multitude of ML-based NIMOR techniques have relied on proper orthogonal decomposition (POD) [8], owing to its robustness and orthogonality. In contrast to it, this paper will employ ANN only for the purpose of order reduction and field reconstruction. Since nonlinear MOR such as variational autoencoder (VAE) and  $\beta$ -VAE [9-11] exhibits superior generative capability when compared against linearized MOR [12], LSH-VAE [13], a variant of VAE will be used. LSH-VAE is characterized by a deep hierarchical architecture integrating a modified loss function. The deep hierarchical structure such as the ladder VAE (LVAE) [14] and Nouveau VAE (NVAE) [15] consist of the multiple layers for a stable network and significant expressiveness. In order to mitigate posterior collapse and enhance the orthogonality of the latent space, the adapted loss function will integrate hybrid weighted least squares and Kullback–Leibler divergence (KLD) [16, 17].

An objective of this paper is to propose a parametric MOR technique for the gust load analysis with the aim of reducing the design period of HALE UAV. Since a HALE UAV operates in straight-and-level flight condition, gust load analysis will be attempted for such flight condition with an objective of enhancing the efficiency and reliability of the design process.

## 2 THEORETICAL BACKGROUND

Prior to a detailed consideration of the formulations of LSH-VAE, it will be better to provide a brief overview of the fundamental characteristics underlying existing ML method. The principal distinctions between the present framework and existing techniques are also presented.

### 2.1 Variational autoencoder (VAE)

VAE is one of the most widely utilized unsupervised generative models, which aims to learn the most salient features of a given dataset without the need for supervision. The VAE is comprised of two networks: an encoder and a decoder as shown in Fig. 1. The decoder is employed to approximate the conditional distribution  $p(x|z)$  for reconstructing the data  $x$  from the prior distribution of the latent space  $p(z)$ . During training, the encoder estimates the variational posterior  $q(z|x)$ , which approximates the latent distribution  $p(z)$ . This distribution is utilized to map the data  $x$ , which is located in a high-dimensional data space, to a low-dimensional feature space also known as latent space.

The learning process can be described as the optimization of a loss function composed of two components: a reconstruction loss function and the KLD loss term. In Eq. (1), the joint log-likelihood such as the cross-entropy function is adopted for the first term. The second term corresponds that forces the posterior distribution  $q(z|x)$  with latent distribution  $p(z)$ .

$$L = \mathbb{E}_{q(z|x)}[\log p(x|z)] - D_{KL}(q(z|x) \parallel p(z)) \quad (1)$$

The reparameterization trick is typically employed in the context of latent space modeling. The latent variables  $z$ , which store reduced high-level features, are formulated as in Eq. (2), using the mean  $\mu$ , the variance  $\sigma$  and a predefined Gaussian distributed noise  $\varepsilon$  [9]. Since the latent variables  $z$  have continuity, learning is conducted through backpropagation.

$$z = \mu + \sigma\varepsilon, \quad \varepsilon \sim N(0,1) \quad (2)$$

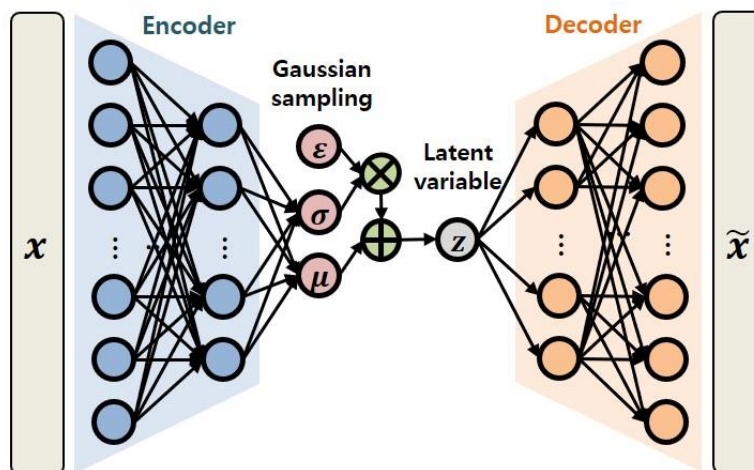


Figure 1: Architecture of VAE.

## 2.2 Least-square hierarchical variational autoencoder (LSH-VAE)

Despite those improvements, vanilla VAE will be prone to vanishing gradients and the loss of long-range correlation due to the limitation of shallow network. It may impede their capacity to represent complex system with numerous number of degrees of freedom. To remedy such limitation, a hierarchically structured deep VAE will be developed as solution to improve performance by preserving long-range correlation and stabilizing the training process. Such structure employs a bidirectional inference network, whereby a bottom-up pass generates feature and the latent variable are processed from top to bottom, with the features shared. In a bidirectional inference network, generation of latent variables will be shared between the two network component. Consequently, KLD loss term will be divided into groups in the loss function of deep hierarchical VAE.

In contrast to the conventional binary cross-entropy KLD, LSH-VAE will employ a hybrid weighted loss function that integrates the mean-squared error (MSE) and KLD. The loss function was empirically demonstrated to yield superior outcomes for continuous result [7]. The loss function of LSH-VAE is shown in Eq. (3).

$$L = \alpha MSE(x, \tilde{x}) - \beta D_{KL}(q(z|x) \parallel p(z)) - \beta \sum_{i=1}^{L-1} \mathbb{E}_{q(z_{<i}|x)} [D_{KL}(q(z_i|z_{<i}, x) \parallel p(z_i|z_{>i}))] \quad (3)$$

In Eq. (3), the  $\alpha$  and  $\beta$  represent the weights for MSE and KLD losses, respectively and the weight ratio is set to approximately  $\alpha: \beta \approx 10^6: 1$ . KL annealing is employed to prevent posterior collapse. In KL annealing, the value of  $\beta$  varies with epochs during training, as illustrated in Eq. (4).

$$\beta = \begin{cases} 1 \times 10^{-4} \beta_{target} & (\text{if } epoch < 0.3n_{epochs}) \\ \beta_{target} \frac{epoch}{n_{epochs}} & (\text{if } epoch > 0.3n_{epochs}) \end{cases} \quad (4)$$

## 3 LSH-VAE OVERVIEW

### 3.1 Architecture of LSH-VAE

As shown in Fig. 2, the encoder and decoder of LSH-VAE comprise of a series of layers, including batch normalization (BN), Swish, spectral normalization (SN), one-dimensional (1D) convolution, exponential linear unit (ELU) and dense. The encoder block output is divided into three paths, one leading to the next block and the other forming  $\mu$  and  $\sigma$ . As illustrated in Fig. 2, additional layers are incorporated into the decoder network to enhance its generative capabilities. The decoder network processes top-down information from preceding decoder block and shared information from latent variable. Then, latent variables and inputs for the subsequent block are generated by the decoder. In order to facilitate bidirectional information sharing, the  $i$ -th shared latent variable  $z_i$  is constructed by combining the  $i$ -th encoder latent variable and the  $(i-1)$ -th decoder latent variable.

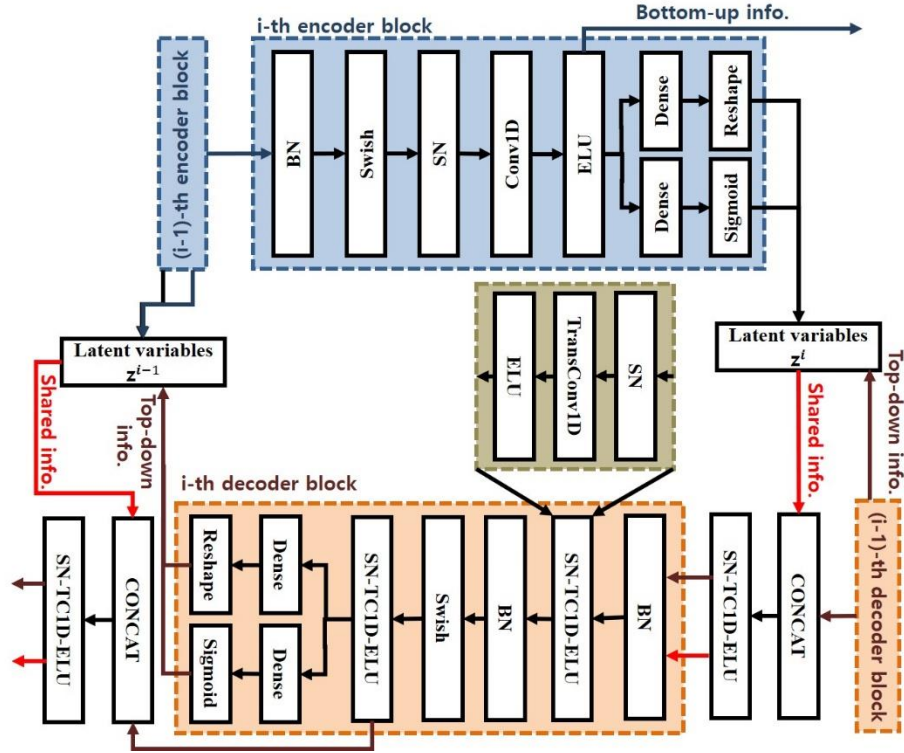


Figure 2: Architecture of the encoder and decoder blocks of LSH-VAE.

### 3.2 Framework of LSH-VAE

Prior to training, the Pre-acquired FOM result is normalized to the range of  $-0.7$  to  $0.7$  for each degree of freedom. The normalized result is augmented by resampling with frequency extension. Then, the original and augmented variables will be concatenated to form the training dataset. In order to enhance the generalization and performance of neural network, the amplitude is adjusted and random noise is added within a range of  $\pm 30\%$  at each epoch.

Subsequently, the encoder network of LSH-VAE compresses the augmented FOM dataset into a latent variable. This will directly facilitate MOR because latent dimension is less than the FOM dimension. Within the training stage, LSH-VAE learns a compressed data representation via gradient-based methods. The Adamax optimizer is adopted for learning parameters of proposed networks. Generative neural networks typically necessitate latent vector exploration due to their probabilistic formulation. However, empirical evidence has demonstrated that with sufficient epochs and a limited number of parameters, such requirement may be eliminated [13]. Instead, the latent vector is computed directly using the mean value of the encoder network.

Subsequently, spherical linear interpolation (slerp) is employed rather than linear linterpolation (lerp) in the latect space. The lerp assumes a straight line between points, which ignores the underlying structure of data distribution. In contrast to it, the slerp will follow the shortest arc on a high-dimensional hypersphere. Since the latent spaces are embedded in high dimensional space, slerp is more appropriate than lerp. The interpolated latent vector is fed to the decoder to reconstruct the target paramter field.

The proposed framework can be divided into two stages: the offline stage and the online stage, as depicted in Fig. 3. Following the construction of FOM dataset for the parametric variations, the offline stage is computed only once and comprises preprocessing and training. Thereafter, the online stage, which contains interpolation and reconstruction, is implemented iteratively for each parametric estimation.

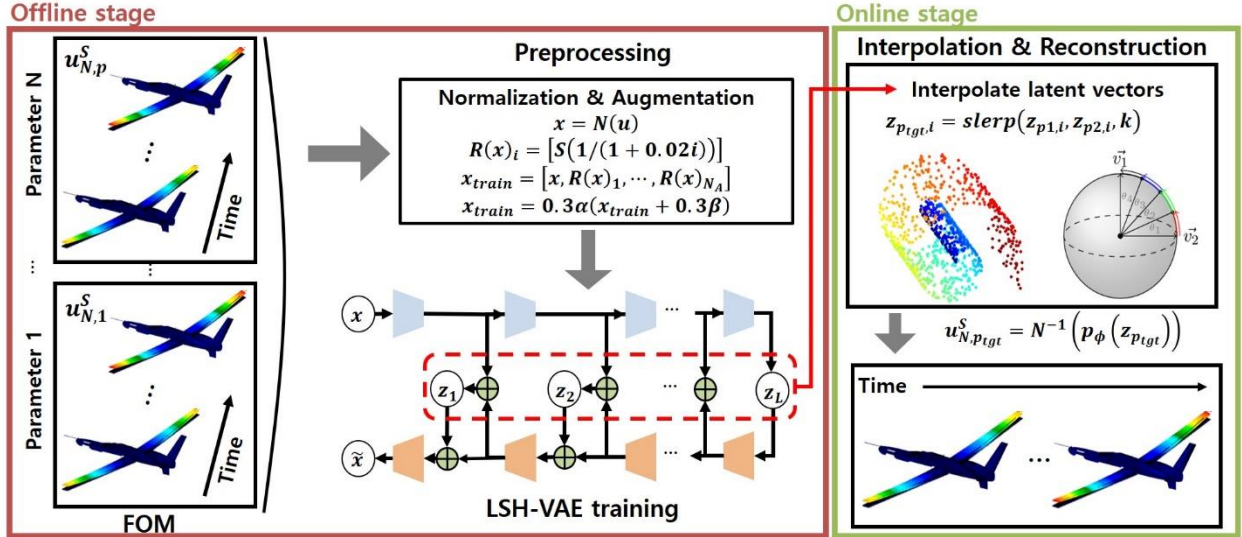


Figure 3: Schematic of LSH-VAE.

## 4 NUMERICAL RESULTS

This section presents the performance of the proposed scheme for HALE UAV subject to gust excitations. A comparison between FOM and current method on target parameter is made, focusing on deformations. The computational time is also compared in terms of speed-up factor.

### 4.1 Gust loads analysis

The gust loads analysis is conducted, which largely follows the gust regulation set forth by FAA [1] and EASA [2]. Twenty parametric samples are extracted based on Latin hypercube sampling, considering altitude, flight speed, gust length, and flight profile alleviation factor. These samples were selected to represent the gust disturbance as 1-cos excitation, and their ranges are summarized in Table 1. DLM, the industry standard for the unsteady aerodynamics, is utilized to compute aerodynamic loads. The generalized mass and stiffness of the HALE UAV, along with the structure eigenvalues and eigenvectors, were obtained from MSC.NASTRAN mode analysis and utilized for the gust simulation. The first four elastic modes are presented in Fig. 4 in the order of the modal frequency. ZAERO is employed to perform gust loads analysis using those parameters and method, thereby ensuring comprehensive and accurate simulation result.

Table 1: Range and unit of the parameter space

Parameter component	Range	Units
Altitude – aircraft height above sea level	[0, 11,000]	m

Flight speed – straight and level flight speed for the aircraft	[70, 80]	m/s
Gust length – the distance for the gust to reach its peak velocity	[9.144, 106.68]	m
Flight profile alleviation factor – scale maximum design gust velocity	[0.6, 1.0]	-

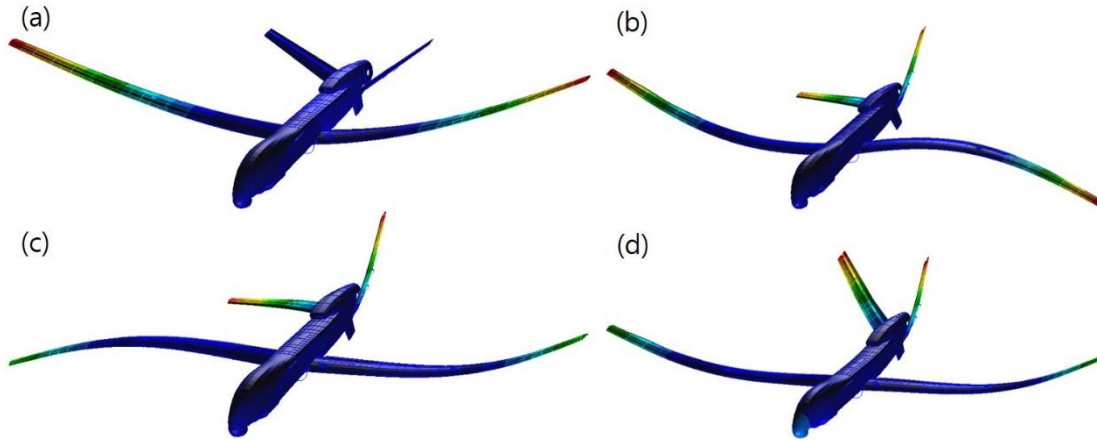


Figure 4: First four elastic modes of the present HALE UAV.

#### 4.2 Structural analysis

As illustrated in Fig. 5, a three-dimensional finite element (FE) discretization of the present HALE UAV is comprised of hybrid elements, including beams, shells and solid elements. The concentrated mass elements are utilized to tune the dynamic behavior of the structural model. The FE model is clamped in the center of gravity region to perform a series of transient simulations. FOM computation is performed by MSC.NASTRAN 2019, by twenty parametric samples. In the context of this paper, the structural analysis is based on the assumption of linear elasticity, including isotropic and orthotropic material. FOM dataset, including the displacement variables  $dx$ ,  $dy$  and  $dz$  is constructed by collecting a 5 second sample of the response at an interval of 0.01 seconds.

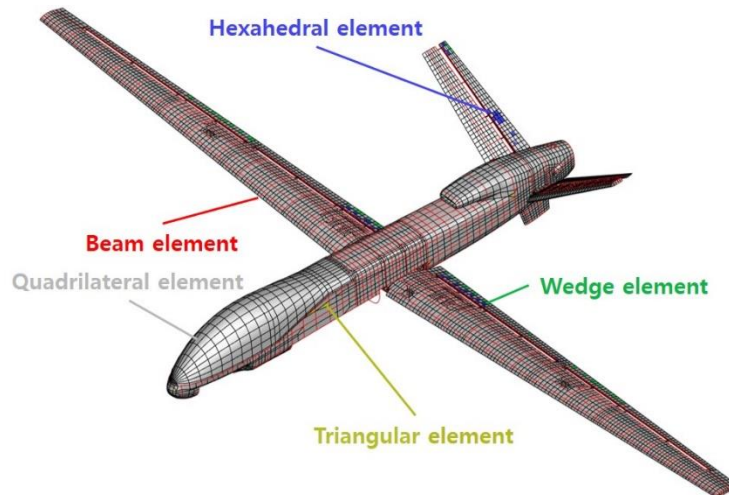


Figure 5: HALE UAV FE discretization.

### 4.3 Parametric MOR using LSH-VAE

FOM dataset is provided to LSH-VAE for training and interpolation. The training of LSH-VAE depends on several hyperparameters, which is summarized in Table 2.

Table 2: Hyperparameters for LSH-VAE

Criterion	Value	Criterion	Value
Epochs $n_{epochs}$	4,000	Latent dimension	[32, 8]
Loss function coefficient $\alpha$	$1 \times 10^6$	Number of filters	[64, 32, 16, 8, 4, 2, 1]
Loss function coefficient $\beta_{target}$	1	Number of resampling augmentations	5
Learning rate	$1 \times 10^{-4}$		

In the present computation, the unknown parameters are selected values at the midpoint in parametric space. Figure 6 illustrates the original and the interpolated deformation field, respectively. To facilitate comparison of the aforementioned field, the coefficient of determination, denoted by  $R^2$ , will be employed.  $R^2$  ranges from zero to one, with higher values indicating more accurate predictions and smaller discrepancies. The formula for  $R^2$  is as follows:

$$R^2 = 1 - \frac{\sum(y - \hat{y})^2}{\sum(y - \bar{y})^2} \quad (5)$$

where  $y$  represents the real values,  $\hat{y}$  the predicted values by LSH-VAE and  $\bar{y}$  the mean of  $y$ . The  $R^2$  value is calculated for each time step, thereby indicating the degree of correlation between the predicted and actual values. Table 3 presents the time-averaged  $R^2$  values for the displacement field. A comparison of the FOM and LSH-VAE results yielded the lowest  $R^2$  value of 0.9713, which may be considered an acceptable outcome.

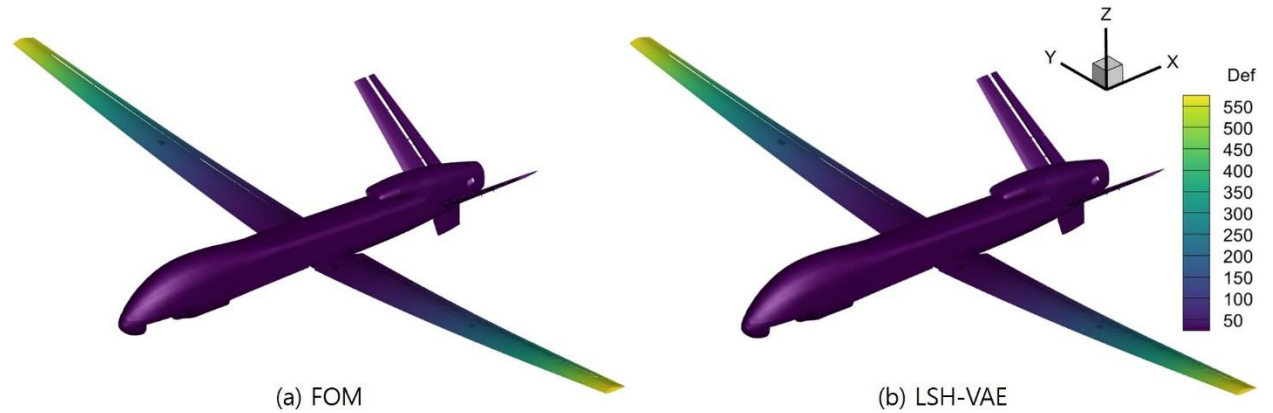


Figure 6: Resultant deflection for the present HALE UAV. All units are in mm.

Table 3: Time-averaged  $R^2$  values of the interpolated displacement field

Variable	$R^2$ value
dx-deflection	0.9851
dy-deflection	0.9713
dz-deflection	0.9732

The computational time consumed for LSH-VAE is also evaluated. The time required for each FOM computation is approximately 1.14 hours per parameter. In total, the offline stage required 22.9 hours, while the online stage requires 0.15 hours. The current approach exhibits a speed-up factor of 7.87 for each unanalyzed parametric estimation. It is concluded that this approach offers significant benefits when the number of computations exceeds 22, as illustrated in Fig. 7.

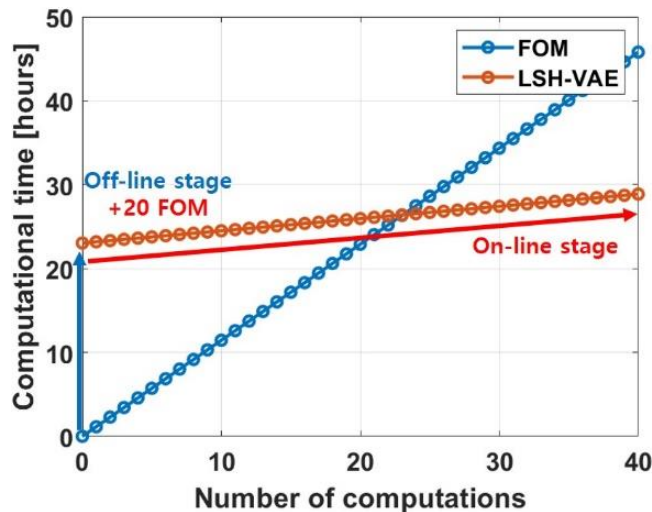


Figure 7: Computational time in terms of parametric queries.

## 5 CONCLUSION

This paper presents an efficient nonlinear parametric NIMOR framework for the gust load analysis. In order to relieve the computational and network training time, Latin Hypercube Sampling and data augmentation are used. The proposed framework is validated using a set of 20 parametric samples on the HALE UAV. Comparison of the result reveals that the current approach exhibited a speed-up factor of 7.87 while achieving high  $R^2$  values of more than 0.97.

In the future, the proposed framework will be applied to maneuver flight, including coordinated turn, climb, and descent. LSH-VAE will be enhanced to accurately reflect the behavior of generalized aeroelastic response in response to variation in the design parameters.

**REFERENCES**

- [1] Anonymous, "Federal Aviation Regulations Part 25," *Airworthiness Standards Transport Category Airplanes* (2014).
- [2] Anonymous, "Certification Specifications and Acceptable Means of Compliance for Large Aeroplanes." (2017).
- [3] Chen, W., et al. "Physics-informed Machine Learning for Reduced-order Modeling of Nonlinear Problems," *Journal of computational physics* 446 (2021): 110666.
- [4] Hesthaven, Jan S., and Ubbiali, S., "Non-intrusive Reduced Order Modeling of Nonlinear Problems using Neural Networks," *Journal of Computational Physics* 363 (2018): 55-78.
- [5] Bertram, A., Othmer, C., and Zimmermann, R., "Towards Real-time Vehicle Aerodynamic Design via Multi-fidelity Data-driven Reduced Order Modeling," *2018 AIAA/ASCE/AHS/ASC Structures, Structural Dynamics, and Materials Conference*. 2018.
- [6] Renganathan, S., Ashwin, Romit M., and Vishwas R., "Machine Learning for Nonintrusive Model Order Reduction of the Parametric Inviscid Transonic Flow past an Airfoil," *Physics of Fluids* 32.4 (2020).
- [7] Lee, S., et al., "Parametric Non-intrusive Model Order Reduction for Flow-fields using Unsupervised Machine Learning," *Computer Methods in Applied Mechanics and Engineering* 384 (2021): 113999.
- [5] Raissi, M., Perdikaris, P., and Karniadakis, G. E., "Physics-informed Neural Networks: A Deep Learning Framework for Solving Forward and Inverse Problems involving Nonlinear Partial Differential Equations," *Journal of Computational physics* 378 (2019): 686-707.
- [6] Regazzoni, F., Dede, L., and Quarteroni, A., "Machine Learning for Fast and Reliable Solution of Time-dependent Differential Equations," *Journal of Computational physics* 397 (2019): 108852.
- [7] Lee, S., et al. "Parametric Model Order Reduction by Machine Learning for Fluid–structure Interaction Analysis," *Engineering with Computers* 40.1 (2024): 45-60.
- [8] Sirovich, L., "Turbulence and the Dynamics of Coherent Structures. I. Coherent Structures," *Quarterly of applied mathematics* 45.3 (1987): 561-571.
- [9] Kingma, P., and Max, W., "Auto-encoding Variational Bayes," *arXiv preprint arXiv:1312.6114* (2013).
- [10] Kneifl, J., et al. "Low-dimensional Data-based Surrogate Model of a Continuum-mechanical Musculoskeletal System based on Non-intrusive Model Order Reduction," *Archive of Applied Mechanics* 93.9 (2023): 3637-3663.
- [11] Wang, Y., et al. "Towards Optimal  $\beta$ -variational Autoencoders Combined with Transformers for Reduced-order Modelling of Turbulent Flows," *International Journal of Heat and Fluid Flow* 105 (2024): 109254.
- [12] Xiang, S., et al. "Non-intrusive Reduced Order Model of Urban Airflow with Dynamic Boundary Conditions," *Building and Environment* 187 (2021): 107397.
- [13] Lee, S., et al. "Data-driven Nonlinear Parametric Model Order Reduction Framework using Deep Hierarchical Variational Autoencoder," *Engineering with Computers* (2024): 1-16.

- [14] Sønderby, K., et al. "Ladder Variational Autoencoders," *Advances in neural information processing systems* 29 (2016).
- [15] Vahdat, A., and Jan K., "NVAE: A Deep Hierarchical Variational Autoencoder," *Advances in neural information processing systems* 33 (2020): 19667-19679.
- [16] Bowman, R., et al. "Generating Sentences from a Continuous Space." *arXiv preprint arXiv:1511.06349* (2015).
- [17] Fu, H., et al. "Cyclical Annealing Schedule: A Simple Approach to Mitigating KL vanishing." *arXiv preprint arXiv:1903.10145* (2019).

### **COPYRIGHT STATEMENT**

The authors confirm that they, and/or their company or organization, hold copyright on all of the original material included in this paper. The authors also confirm that they have obtained permission from the copyright holder of any third-party material included in this paper to publish it as part of their paper. The authors confirm that they give permission, or have obtained permission from the copyright holder of this paper, for the publication and public distribution of this paper as part of the IFASD 2024 proceedings or as individual off-prints from the proceedings.